Available online at www.sciencedirect.com
SCIENCE DIRECT®
International Journal of Heat and Mass Transfer 49 (2006) 3568–3582
International Journal of HEAT and MASS TRANSFER
www.elsevier.com/locate/ijhmt

Conjugate mixed convection with surface radiation from a horizontal channel with protruding heat sources

B. Premachandran, C. Balaji *

Heat Transfer and Thermal Power Laboratory, Department of Mechanical Engineering, Indian Institute of Technology Madras, Chennai 600 036, India

Received 13 April 2005; received in revised form 15 February 2006
Available online 11 May 2006

Abstract

A numerical investigation of conjugate convection with surface radiation from horizontal channels with protruding heat sources has been carried out. The flow is assumed to be steady, laminar, incompressible, hydrodynamically and thermally developing. Air is considered as the working fluid. The geometric parameters such as spacing between the channel walls, size of the protruding heat sources, thickness of the substrate and the spacing between the heat sources are fixed. Results are presented to show the effect of parameters such as Re_S, Gr_S^*, k_p/k_f, k_s/k_f, ε_p and ε_s on the fluid flow and heat transfer. A correlation for the non-dimensional maximum temperature is also developed using the method of asymptotic expansions.

Keywords: Conjugate mixed convection; Surface radiation; Horizontal channel; Protruding heat sources

1. Introduction

Rapid advances in semiconductor technology have lead to increase in miniaturization in circuit design and hence the amount of heat that must be dissipated per unit volume of a device continues to increase enormously. Air is a preferred coolant because of easy handling, easy maintenance and reliability. Forced convection air-cooling is used if the heat flux from the component is more than 1000 W/m^2. Even if the flow is a forced one, the effect of buoyancy is not negligible when the heat flux from the electronic chip is very high. Hence, the flow may be in the mixed convection regime. It is important to consider the effects of conjugateness and surface radiation when analyzing a mixed convection problem, to accurately predict the fluid flow and heat transfer characteristics, as for example the cooling of electronic components, when air is considered as a cooling medium.

Davalath and Bayazitolgu [1] presented results of a numerical study of conjugate forced convection air-cooling of three protruding heat sources mounted on a horizontal channel. To study the effect of conduction in the substrate, both finite thick wall and adiabatic wall were considered as substrate. The effect of Reynolds number on the fluid flow and heat transfer was analyzed and the results were also presented for the effect of Prandtl number. Kim and Anand [2] carried out a numerical investigation of forced convection conjugate heat transfer from protruding heat sources, considering a uniform profile at the inlet. A periodic boundary condition was used at the outer surface of the substrate to simulate a large number of circuit boards arranged in the transverse direction. Young and Vafai [3] also carried out a detailed numerical study of conjugate forced convection in a channel with protruding heat sources. Very recently, Furukawa and Young [4] also carried out a numerical study of forced convection from a horizontal channel with protruding heat sources. Kim et al. [5] carried out a numerical study of fluid flow and heat transfer characteristics of mixed convection in a channel with protruding heat sources mounted on the bottom channel wall.

* Corresponding author. Tel.: +91 22574689; fax: +91 22570509.
E-mail address: balaji@iitm.ac.in (C. Balaji).

0017-9310/$ - see front matter © 2006 Published by Elsevier Ltd.
doi:10.1016/j.ijheatmasstransfer.2006.02.044

Nomenclature

A	aspect ratio, (L/S) or (d/H), problem specific
b	spacing between the heat sources, m
c	specific heat, J/kg K
d	cavity width, m
F_{ij}	view factor from ith element to the jth element of an enclosure
g	acceleration due to gravity, 9.81 m/s^2
Gr_S^*	modified Grashof number, based on volumetric heat generation, $g\beta\Delta T_{\text{ref}}S^3/\nu^2$
H	cavity height, m
J	radiosity, W/m^2
J^*	non-dimensional radiosity, $J/\sigma T_\infty^4$
k	thermal conductivity, W/mK
L_{h},t_{h}	width and height of the protruding heat source, respectively, m
L	length of the channel, m
L_{e}	non-dimensional length of the extended domain
p	pressure at any location in the computational domain, Pa
P	non-dimensional pressure at any location in the computational domain
Pe_S	Peclet number based on S, $u_\infty S/\alpha$
Pr	Prandtl number, ν/α
q_{v}	volumetric heat generation from the protruding heat sources, W/m^3
$q_{\text{R},i}$	non-dimensional elemental radiative heat flux, defined in Eq. (8)
Ra_H	Rayleigh number, $g\beta(T_{\text{h}}-T_\infty)H^3/\nu\alpha$
Re_S	Reynolds number based on S, $u_\infty S/\nu$
Ri_S^*	modified Richardson number based on S, (Gr_S^*/Re_S^2) or $(g\beta\Delta T_{\text{ref}}S/u_\infty^2)$
S	spacing between the channel walls, m
t'	time, s
t	thickness of the channel wall, m
t_{h}	thickness of the heat source, m
T_∞	free stream or entry temperature of the fluid, K
T_{h}	temperature of the hot wall of the cavity, K
T	temperature at any location in the computational domain, K
u_∞	free stream velocity, m/s
u	horizontal velocity, m/s
U	non-dimensional horizontal velocity, u/u_∞
v	vertical velocity, m/s
V	non-dimensional vertical velocity, v/u_∞
w	height of the side vent, m
W	non-dimensional height ratio of the side vent (w/H)
x, y	horizontal and vertical distances, respectively, m
X, Y	non-dimensional horizontal and non-dimensional vertical distances, x/S, y/S, respectively

Greek symbols

α	thermal diffusivity of the fluid, m^2/s
β	isobaric cubic expansivity of the fluid, $-\frac{1}{\rho}\left(\frac{\partial\rho}{\partial T}\right)_P$, 1/K
δ	convergence criterion, in fractional form, $\lvert(\zeta_{\text{new}}-\zeta_{\text{old}})/\zeta_{\text{new}}\rvert$
ε	surface emissivity
ϕ_1, ϕ_2, ϕ_3, ϕ_4, ϕ_5, ϕ_6	parameters in the asymptotic expansion
ν	kinematic viscosity of fluid, m^2/s
θ	non-dimensional temperature at any location in the computational domain, $(T-T_\infty)/\Delta T_{\text{ref}}$
σ	Stefan–Boltzmann constant, 5.6697×10^{-8} W/m^2 K^4
τ	non-dimensional time, $u_\infty t'/S$
ζ	any variable (U, V, θ and J^*) over which convergence is being tested for

Subscripts

f	fluid
h	heat source
max	maximum
new, old	values of the dependent variables (U, V, θ and J^*) obtained from the present and previous iterations
p	protruding heat source
ref	reference value
s	channel wall or substrate (problem specific)
∞	ambient

Miscellaneous symbols

ΔT_{ref}	modified reference temperature difference $(q_{\text{v}}L_{\text{h}}t_{\text{h}}/k_{\text{f}})$ or (T_H-T_C), K
Δx	width of the element chosen for energy balance, m
ΔX	non-dimensional width of the element chosen for energy balance, $\Delta x/S$
Δy	height of the element chosen for energy balance, m
ΔY	non-dimensional height of the element chosen for energy balance, $\Delta y/S$

But all of the above studies, whether for conjugate forced convection or mixed convection from channels with protruding heat sources, have neglected the effect of radiation heat transfer altogether. However, a few studies on conjugate convection with surface radiation from geometries applicable to electronic circuit boards with chips have demonstrated that the effect of radiation is not negligible. Smith et al. [6] presented results of a numerical investigation of conjugate natural convection with surface radiation in an electronic chassis consisting of an

enclosure, containing three printed circuit boards on which heat generating components of various sizes were mounted. A detailed parametric study was carried out to investigate the effect of conduction, convection and radiation heat transfer for various thermo-physical properties, such as thermal conductivities of the wall, heat sources and guard guide and the emissivities of components and walls.

Lee et al. [7] carried out an analysis of conjugate mixed convection with surface radiation from a plate, with two isoflux heat sources mounted inline with the vertical plate. Balaji and Venkateshan [8] carried out a detailed numerical study of conjugate natural convection with surface radiation from a slot where both the vertical walls were conducting and the bottom wall was isothermal. Various Rayleigh numbers, thermal conductivities, emissivities and aspect ratios were considered, while conducting the parametric study. A correlation was given for the average Nusselt number by taking into account all the pertinent parameters. Dehghan and Behnia [9], numerically, investigated combined conduction and natural convection with surface radiation from a top open cavity with a discrete constant flux source mounted on the left sidewall of finite thickness. Flow visualization studies were also carried out. A parametric study was conducted for a fixed set of geometric parameters and a fixed thermal conductivity ratio.

Yu and Joshi [10] carried out both numerical and experimental investigations of combined conduction, natural convection and surface radiation from a side vented enclosure with a discrete heat source mounted at the middle of a vertical substrate. All the geometric parameters were fixed, except the side opening. To study the effect of radiation heat transfer, the emissivity of substrate was changed from 0 to 1. A parametric study was carried out for two Rayleigh numbers, $Ra = 2.6 \times 10^6$ and 2.6×10^7. Adams et al. [11] carried out a numerical analysis of conjugate natural convection with surface radiation from an enclosure (aspect ratio of 6:1) with 3×3-heat sources mounted on a substrate. The study examined the complex thermal interactions between the heat sources, substrate and enclosure walls.

Liu and Phan-thien [12], numerically, investigated conjugate natural convection with surface radiation heat transfer in a differentially heated square cavity and a volumetric heat generating heat source placed at the middle of the cavity. They included the effect of shadowing while calculating the radiation heat transfer.

Gururaja Rao et al. [13] presented results of conjugate mixed convection with surface radiation from a vertical channel with two flush mounted heat sources mounted on each of the channel walls. Results were presented for a wide range of parameters such as Reynolds number, Richardson number, emissivity of right and left sidewalls, conductivity of channel walls (including heat sources) and aspect ratios. Joseph et al. [14] experimentally investigated cooling of heated modules simulating electronic components for the following conditions: single component cooled by natural convection, single component cooled by forced convection, multiple components cooled by natural convection, multiple components cooled by forced convection. The pitch and absorptivity of PCBs, aspect ratio, and emissivity of electronic components were considered as parameters, while conducting the experiments.

From the literature survey, it is clear that the effect of radiation on conjugate mixed convection with surface radiation from channels with protruding heat sources has not been studied. Hence, a numerical analysis of conjugate mixed convection from a horizontal channel with four volumetrically heat generating heat sources mounted on the bottom channel wall with a view to investigate the effect of buoyancy and surface radiation is attempted in this study. A correlation for the non-dimensional maximum temperature is also developed, based on asymptotic expansions.

2. Statement of the problem and method of solution

The schematic view of the geometry considered in the present study is given in Fig. 1. Four heat sources each with a volumetric heat generation q_v of length L_h and height t_h are mounted on the bottom wall of the channel of thickness t and length L. The length and thickness of the top wall of the channel are same as that of the bottom wall. The thermal conductivity (k_p) and the emissivity (ε_p) of the heat sources and those of the channel wall thermal conductivity (k_s) and emissivity (ε_s) are different from each other. The inlet, exit faces and the outer surfaces of the channel walls are assumed to be adiabatic.

The principal objective of the present work is to study the effect of thermal parameters. Hence, the geometric parameters are fixed throughout the parametric study. The dimensions considered in the present study are as follows: $L = 300 \times 10^{-3}$ m, $t = 2.5 \times 10^{-3}$ m, $S = 25 \times 10^{-3}$ m, $t_h = 7.5 \times 10^{-3}$ m, $L_h = 15 \times 10^{-3}$ m, $b = 10 \times 10^{-3}$ m. The first heat source is mounted at a distance of 0.05 m from the leading edge of the bottom channel wall. Air is considered as a working fluid and is assumed to be a non-participating medium. The flow is assumed to be laminar, incompressible, hydrodynamically and thermally developing. The medium is assumed to have constant properties, outside of density, for which the Boussinesq approximation is assumed to hold good. Based on the above-mentioned assumptions, the non-dimensional form of the governing equations for the fluid side can be written as follows:

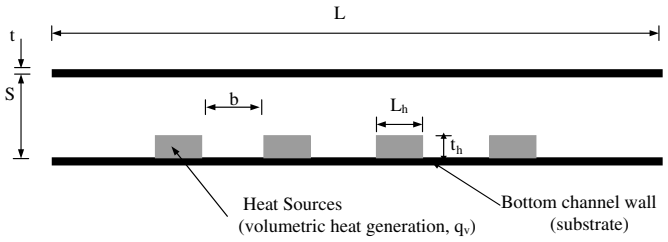

Fig. 1. Schematic view of the problem.

Continuity

$$\frac{\partial U}{\partial X}+\frac{\partial V}{\partial Y}=0 \tag{1}$$

X-momentum

$$\frac{\partial U}{\partial \tau}+U\frac{\partial U}{\partial X}+V\frac{\partial U}{\partial Y}=-\frac{\partial P}{\partial X}+\frac{1}{Re_S}\left(\frac{\partial^2 U}{\partial X^2}+\frac{\partial^2 U}{\partial Y^2}\right) \tag{2}$$

Y-momentum

$$\frac{\partial V}{\partial \tau}+U\frac{\partial V}{\partial X}+V\frac{\partial V}{\partial Y}=-\frac{\partial P}{\partial Y}+\frac{1}{Re_S}\left(\frac{\partial^2 V}{\partial X^2}+\frac{\partial^2 V}{\partial Y^2}\right)+\frac{Gr_S^*}{Re_S^2}\theta \tag{3}$$

Energy

$$\frac{\partial \theta}{\partial \tau}+U\frac{\partial \theta}{\partial X}+V\frac{\partial \theta}{\partial Y}=\frac{1}{Re_S Pr}\left(\frac{\partial^2 \theta}{\partial X^2}+\frac{\partial^2 \theta}{\partial Y^2}\right) \tag{4}$$

Energy equation for the solid region

Channel walls

$$Pe_S\left(\frac{\rho_s c_s}{\rho_f c_f}\right)\frac{\partial \theta}{\partial \tau}=\frac{k_s}{k_f}\left(\frac{\partial^2 \theta}{\partial X^2}+\frac{\partial^2 \theta}{\partial Y^2}\right) \tag{5}$$

Heat sources

$$Pe_S\left(\frac{\rho_p c_p}{\rho_f c_f}\right)\frac{\partial \theta}{\partial \tau}=\frac{k_p}{k_f}\left(\frac{\partial^2 \theta}{\partial X^2}+\frac{\partial^2 \theta}{\partial Y^2}\right)+\frac{S^2}{L_h t_h} \tag{6}$$

2.1. Calculation of radiative heat transfer

Calculation of radiation heat transfer is carried out using the radiosity/irradiation formulation. The interior surfaces of the enclosure are assumed to be opaque, diffuse and gray. The openings (channel inlet and outlet) are assumed to be black at the ambient temperature. The general non-dimensional radiosity equation for the ith element of the enclosure, which is filled with a radiatively non-participating medium, like air, may be written as

$$J_i^*=\varepsilon_i\left(\frac{T_i}{T_\infty}\right)^4+(1-\varepsilon_i)\sum_{j=1}^{n}J_j^* F_{ij} \tag{7}$$

Here, ε_i is the hemispherical, total emissivity of any element i, which is assumed to be at uniform temperature T_i. F_{ij} is the view factor (or shape factor) from the ith element to the jth element of the enclosure, while n is the total number of elements along the boundaries of the enclosure. For this problem, the enclosure consists of the inlet, outlet of the channel and the solid to fluid interfaces. The total number of small elemental surfaces taken for the radiation calculations is equal to the sum of interface nodal points, nodal points at the fluid inlet boundary and nodal points at the fluid exit of the channel plus (5×4). The latter one is taken into account as corner points are common for two surfaces and there are four corner points at the four protruding heat sources in addition to the four corner points of the radiation computation domain. The extended domain is not included, for the sake of reducing the computational effort and time. Based on the radiosity and irradiation formulation, the dimensionless radiative flux from the discrete surface "i" is given by

$$q_{R,i}=\frac{\varepsilon_i}{1-\varepsilon_i}\left[\left(\frac{T_i}{T_\infty}\right)^4-J_i^*\right] \tag{8}$$

where $J^*=\dfrac{J}{\sigma T_\infty^4}$.

To calculate the view factors between two surfaces with and without obstructions, Hottel's crossed string method [15] is used.

2.2. Calculation of temperature at the interface nodal points

Interface temperature values are calculated by carrying out energy balance as follows:

(a) For the channel walls and fluid interface:

$$-\frac{k_s}{k_f}\left(\frac{\partial \theta}{\partial Y}\right)_s=-\left(\frac{\partial \theta}{\partial Y}\right)_f+N_{RC}q_R \tag{9}$$

where

$$N_{RC}=\frac{\sigma T_\infty^4}{k_f}\frac{S}{\Delta T_{ref}}$$

(b) For the heat source and fluid interface:
To calculate the temperature values at the interface of heat source and fluid, half control volumes (or quarter control volumes for the corner nodes), to take the volumetric heat generation into account, are taken and an energy balance is carried out. The equation, based on energy balance, for the interface nodal point located on the horizontal surface of the heat sources is as follows:

$$-\frac{k_p}{k_f}\left(\frac{\partial \theta}{\partial X}\right)_w\Delta Y-\frac{k_p}{k_f}\left(\frac{\partial \theta}{\partial Y}\right)_s\Delta X+\left(\frac{\partial \theta}{\partial Y}\right)_n\Delta X+\frac{k_p}{k_f}\left(\frac{\partial \theta}{\partial X}\right)_e+\frac{S^2}{L_h t_h}\Delta X\Delta Y-N_{RC}q_R\Delta X=Pe_S\frac{\partial \theta}{\partial \tau}\Delta X\Delta Y \tag{10}$$

2.3. Boundary conditions

The computational domain along with the boundary conditions is shown in Fig. 2. Taking the outlet of the channel as a computational domain boundary will lead to unrealistic results, because of a large re-circulation after the last heat source. Hence, an extended domain is used at the outlet of the channel to avoid any influence by the downstream boundary conditions.

Adiabatic boundary condition is imposed on the outer surfaces of the channel walls:

Inlet boundary conditions

The fluid is assumed to enter the channel with uniform velocity and temperature profiles, and the appropriate boundary conditions are

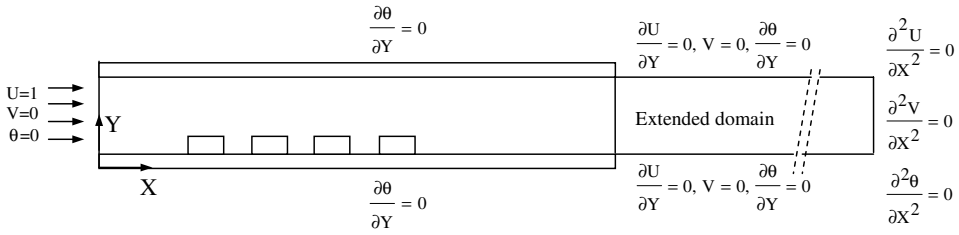

Fig. 2. Computational domain and the boundary conditions.

$$U = 1.0 \tag{11}$$

$$V = 0 \tag{12}$$

$$\theta = 0 \tag{13}$$

Outlet boundary conditions

For the outlet of the computational domain, the following boundary conditions are used:

$$\frac{\partial^2 U}{\partial X^2} = 0; \quad \frac{\partial^2 V}{\partial X^2} = 0; \quad \frac{\partial^2 \theta}{\partial X^2} = 0 \tag{14}$$

For the top and bottom of the extended computational domain, the following boundary conditions are imposed:

$$\frac{\partial U}{\partial Y} = 0 \tag{15}$$

$$V = 0 \tag{16}$$

$$\frac{\partial \theta}{\partial Y} = 0 \tag{17}$$

2.4. Solution procedure

The governing equations for fluid and solid regions are solved using a finite volume method. SIMPLE algorithm [16] is used to couple velocity and pressure. A point-by-point Gauss–Siedel iteration is used to solve for U, V, θ and J^*. A convergence criterion, δ, of 1×10^{-5} has been imposed for all the variables U, V, θ and J^*.

2.5. Validation

To validate the code for conjugate heat transfer, the present results were compared with those of Kaminsky and Prakash [17] for conjugate natural convection in a square cavity. The detailed comparison of the present results with those of Kaminsky and Prakash is given in Premachandran and Balaji [18]. To validate the code for the combined convection and radiation interaction, the results of the present study were compared with the experimental results of Ramesh and Merzkirch [19] for combined natural convection and radiation in a side vented open cavity. Results were compared for the percentage heat transfer contribution by convection and radiation for an aspect ratio, $A = 0.5$ and a dimensionless width, $W = 0.5$ for a wide range of Rayleigh numbers and two emissivity values 0.05 and 0.85 (Fig. 3). From the figure, it is clear that the results of the present study agree very well with those of Ramesh and Merzkirch.

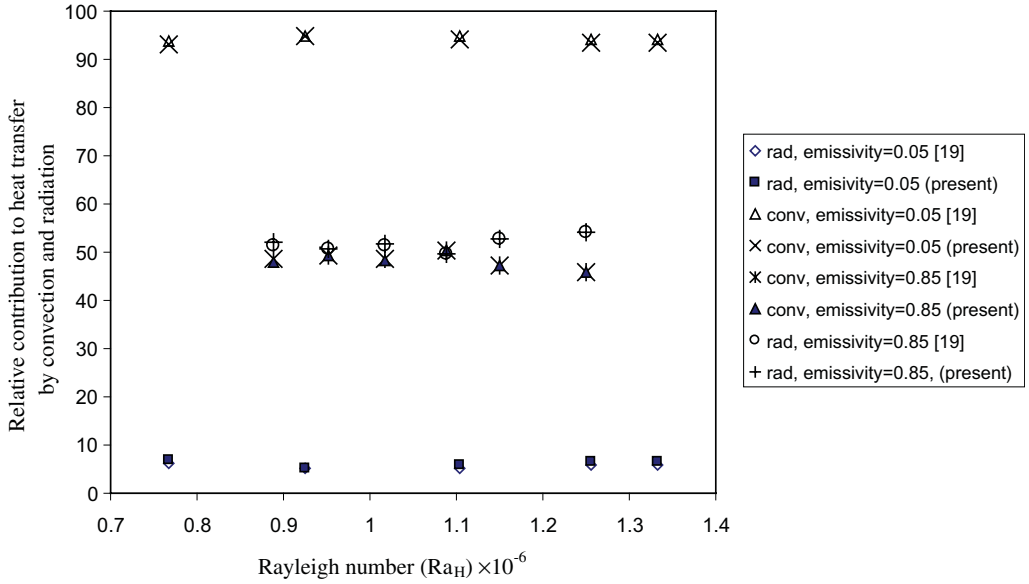

Fig. 3. The effect of surface emissivity of the left wall on contribution to convection and radiation heat transfer for various Ra_H of the side vented open cavity.

3. Results and discussion

3.1. Range of parameters considered

The geometric parameters are fixed while carrying out the parametric study. A detailed parametric study has been carried out to investigate the effects of Re_S, Gr_S^*, k_s/k_f, k_p/k_f, ε_p and ε_s. The emissivity of the channel walls and heat sources are varied from 0.02 to 0.85. (The emissivities of the polished aluminum foil and black paint are 0.05 and 0.85, respectively.) Smith et al. [6] considered anisotropic conduction within the substrate with $k_x = 3.03 - 3.47$ W/mK and $k_y = 4.86 - 56.2$ W/mK. In the present study, the effective thermal conductivity value of substrate (k_S) is varied from 1.3 W/mK to 13 W/mK, considering isotropic conduction within the channel walls (substrate). The same range is also used for the thermal conductivity of heat sources (k_p). The range of parameters considered for the present study is given in Table 1. The baseline case considered for the present study has the following set of thermal parameters: $Re_S = 500$, $Gr_S^* = 8.65 \times 10^5$, $k_p/k_f = 100$, $k_s/k_f = 50$, $\varepsilon_p = 0.55$ and $\varepsilon_s = 0.55$.

3.2. Grid independence study

In order to obtain grid independent solutions, a grid independence study was carried out. A non-uniform grid is used for throughout the domain. Very fine grids are used near the walls. The effect of extended domain length (L_e) and the number of grid points on the non-dimensional maximum temperature was carried out by checking the flow pattern and the variation in the non-dimensional maximum temperature for both low and high Reynolds number flows. Based on this study, a non-dimensional length, $L_e = 8$ is fixed with 120 points along the X-direction for all the subsequent calculations.

The details of the results of the grid independence study are given in Table 2. When the total number of grid points used for the computations increased from 32,752 to 43,186, a change of only 0.104% was observed on the non-dimensional maximum temperature. Hence, a grid size of 32,752 is used for the range of parameters considered in the present study.

Table 1
Range of parameters used in the present study ($T_\infty = 300$ K, $Pr = 0.71$, $A = 12$)

$250 \leqslant Re_S \leqslant 1000$
$6.5 \times 10^4 \leqslant Gr_S^* \leqslant 4.33 \times 10^6$
$7.5 \times 10^4 \leqslant q_v \leqslant 5 \times 10^5$ (W/m^3)
$50 \leqslant k_p/k_f \leqslant 500$
$50 \leqslant k_s/k_f \leqslant 500$
$0.02 \leqslant \varepsilon_p \leqslant 0.85$
$0.02 \leqslant \varepsilon_s \leqslant 0.85$

Table 2
Results of the grid independence study for $Re_S = 750$, $Gr_S^* = 8.65 \times 10^5$, $q_v = 1 \times 10^5$ W/m^3, $k_p/k_f = 100$, $k_s/k_f = 50$, $\varepsilon_p = 0.55$, $\varepsilon_s = 0.55$

No. of nodal points	θ_{max}	Percentage change
13,050	0.079	–
21,170	0.0838	5.72
32,752	0.08582	2.35
43,186	0.08591	0.104

3.3. Effect of Reynolds number

Fig. 4 shows the streamline pattern for $Re_S = 250$, 500 and 1000. The fluid between the cavities is driven by the shear stress due to the core flow, which is similar to the classical lid driven cavity flow, where the moving lid drives the flow in the cavity. As the Reynolds number increases, the center of the circulation in the cavities shifts towards the right side wall of the cavities. Beyond the last protruding heat source, the length and relative strength of the re-circulation increases, as the Reynolds number increases. The temperature distribution is shown in Fig. 5 for $Re = 250$, 500 and 1000 while all the other parameters are at the baseline values. As the fresh air has contact with the first chip, the convective heat transfer is high and hence the temperature of the first chip is lower than the other chips. The maximum temperature of the last chip is less than the penultimate chip because of the large re-circulation carries away heat from the last chip to the core flow. Apart from convection, the first and last chips are exposed to the open atmosphere and the radiation heat transfer from these chips is high compared to the interior chips. Because of radiation interaction, a radiation induced thermal boundary layer forms at the top channel wall. As the Re_S increases, the effect of radiation decreases and the thermal boundary layer becomes less pronounced. As expected, the non-dimensional maximum temperature decreases as the Reynolds number increases. The variation of non-dimensional maximum temperature with respect to Reynolds number is given in Fig. 6.

To develop a correlation for the non-dimensional maximum temperature in the channel, θ_{max}, using the method

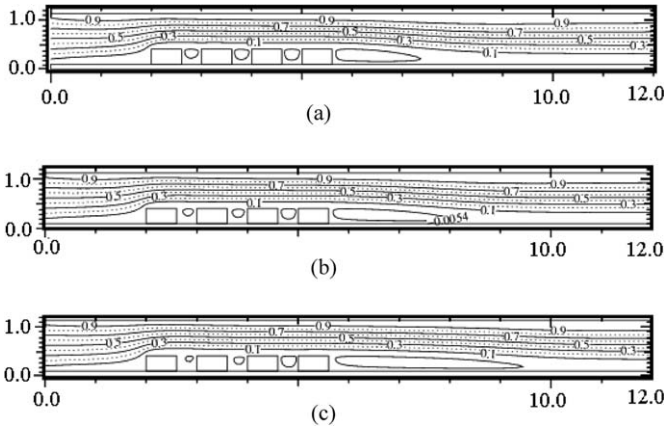

Fig. 4. Streamline plots for various Reynolds number, Re_S: (a) $Re_S = 250$, (b) $Re_S = 500$, (c) $Re_S = 1000$.

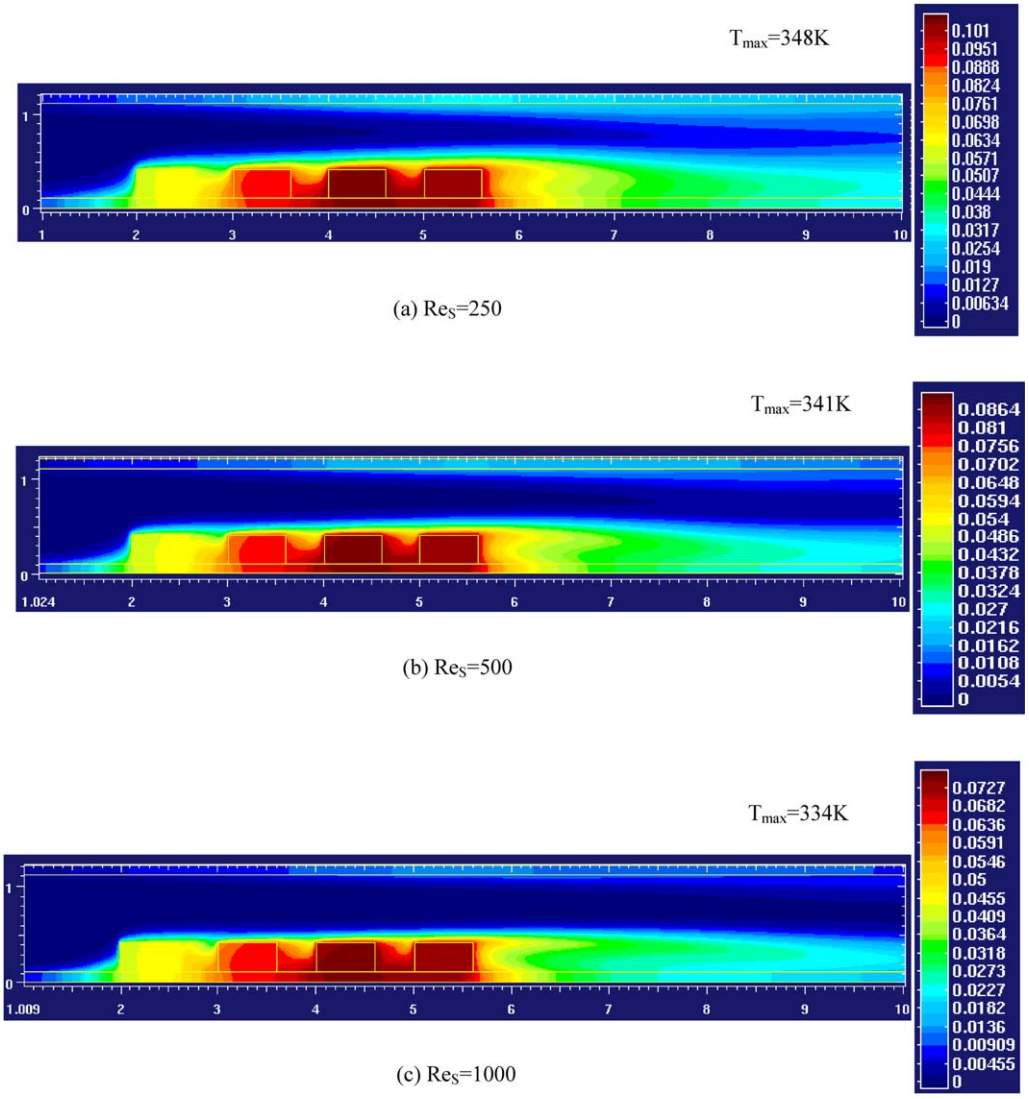

Fig. 5. Effect of Reynolds number on the temperature distribution $Gr_S^* = 8.65 \times 10^5$, $q_v = 1 \times 10^5$ W/m^3, $k_s/k_f = 50$, $k_p/k_f = 100$, $\varepsilon_s = 0.55$, $\varepsilon_p = 0.55$.

of asymptotic expansions, a linearised curve is obtained for θ_{max} with respect to $(Re_S/Re_{S,ref})^{0.22}$. In this study, the baseline parameters are taken as the reference parameters to develop the correlation. Hence, $Re_{S,ref} = 500$, $Gr^*_{S,ref} = 8.65 \times 10^5$, $(k_p/k_f)_{ref} = 100$, $(k_s/k_f)_{ref} = 50$, $\varepsilon_{p,ref} = 0.55$ and $\varepsilon_{s,ref} = 0.55$. Similar linearised curves are also plotted for other parameters, wherever required.

3.4. Effect of modified Grashof number, Gr_S^*

To investigate the effect of buoyancy, the values of volumetric heat generation (q_v) are changed to obtain different modified Grashof number values, Gr_S^*. There is no change in flow pattern for the range of modified Grashof number considered in the present study. This fact is also evident from Fig. 7, which shows a linear variation of the non-dimensional maximum temperature with modified Grashof numbers. (Since the definition of reference temperature difference in the non-dimensional temperature is written in terms of q_v and the source term in the non-dimensional energy equation contains only the geometric parameters, for forced convection flow calculations, solving the governing equations by neglecting buoyancy term, one needs only one run to obtain different dimensional temperature distributions for different q_v values for a particular Reynolds number.) Fig. 7 also shows that the non-dimensional temperature decreases as the Gr_S^* increases. However, the dimensional temperature increases as Gr_S^* increases, for reasons already explained.

3.5. Effect of emissivity of heat sources and channel walls

Fig. 8 shows the effect of the emissivity of the heat source on the temperature distribution, when other parameters are fixed at the baseline values. As the emissivity of the heat sources, ε_p, increases from 0.02 to 0.85 and the other values are at the baseline values, the maximum temperature decreases from 346 K to 342 K, because of an increase in radiation heat transfer. As the radiation heat transfer from heat source increases, the interaction between

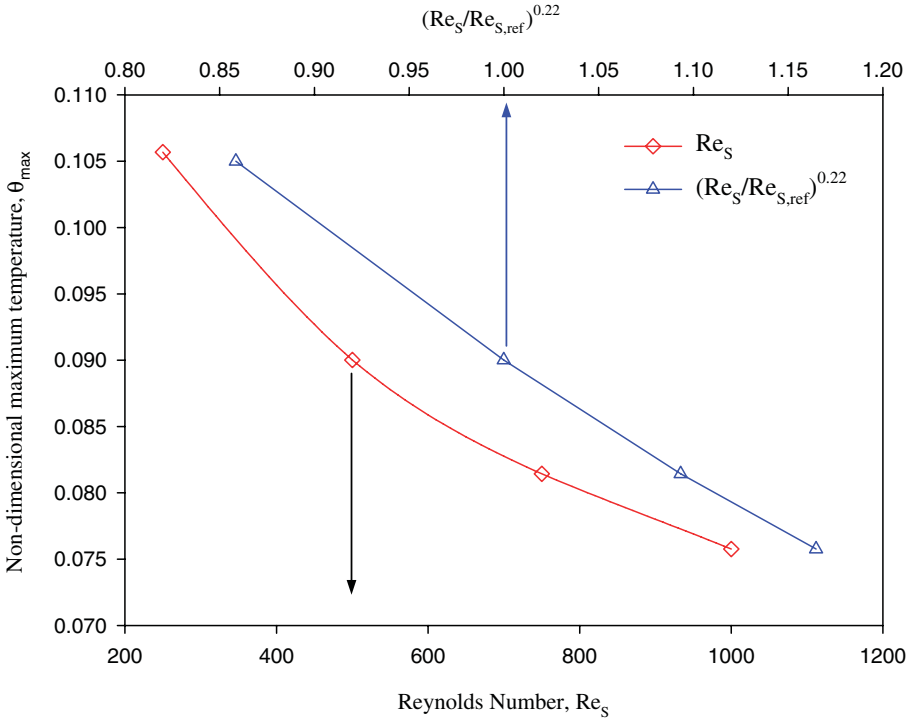

Fig. 6. Effect of Reynolds number on the non-dimensional maximum temperature.

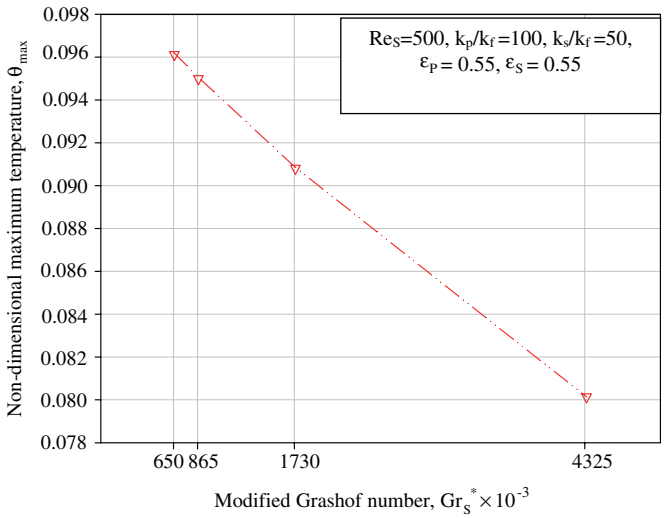

Fig. 7. Effect of modified Grashof number on the non-dimensional maximum temperature.

top wall and the heat source also increases. The change in non-dimensional maximum temperature with change in emissivity of heat sources for $Re_S = 250$,500 and 1000 is given in Fig. 9.

The effect of the emissivity of the channel walls, ε_s on the heat transfer characteristics is also investigated. Fig. 10 shows the effect of the emissivity of the channel walls on the temperature distribution for $\varepsilon_s = 0.02$, 0.3 and 0.85. The other values are kept at baseline parametric values. Fig. 11 shows the effect of emissivity of the channel walls ε_s on the non-dimensional maximum temperature for various Reynolds numbers.

As the ε_s increases, the temperatures inside the channel decrease. Because of increase in radiation interaction by the top channel wall surface, the temperature of the top wall increases. Due to this, the convective heat transfer increases from the top channel wall as the emissivity of the top wall increases. When the emissivity of the substrate changes from 0.02 to 0.85, while other parameters are fixed at reference values, a 11 °C drop in the maximum temperature is observed. On the other hand, only a 4 °C drop in maximum temperature is observed when ε_p is changed from 0.02 to 0.85. From the above analysis, it is clear that the effect of the emissivity of the channel walls is more significant than the emissivity of the heat sources. Fig. 12(a) shows the temperature distributions on the top surface of the bottom channel. Because of the low temperatures at the upstream side of the first protrusion, the effect of ε_s is negligible compared to the downstream side of the last protruding heat source.

The temperature distributions at the interface between the top channel wall and fluid are shown in Fig. 12(b) for different emissivity values of the channel walls (ε_s). As the emissivity of the channel walls increases, the radiation interaction increases. Hence, the top surface temperature of the top channel (cold) wall increases. Due to this reason, the convective heat transfer from the top channel wall also increases. At the leading edge of the top channel wall, the radiation interaction is negligible compared to the middle of the top channel wall. Furthermore, the fresh air cools the leading portion of the top channel wall considerably.

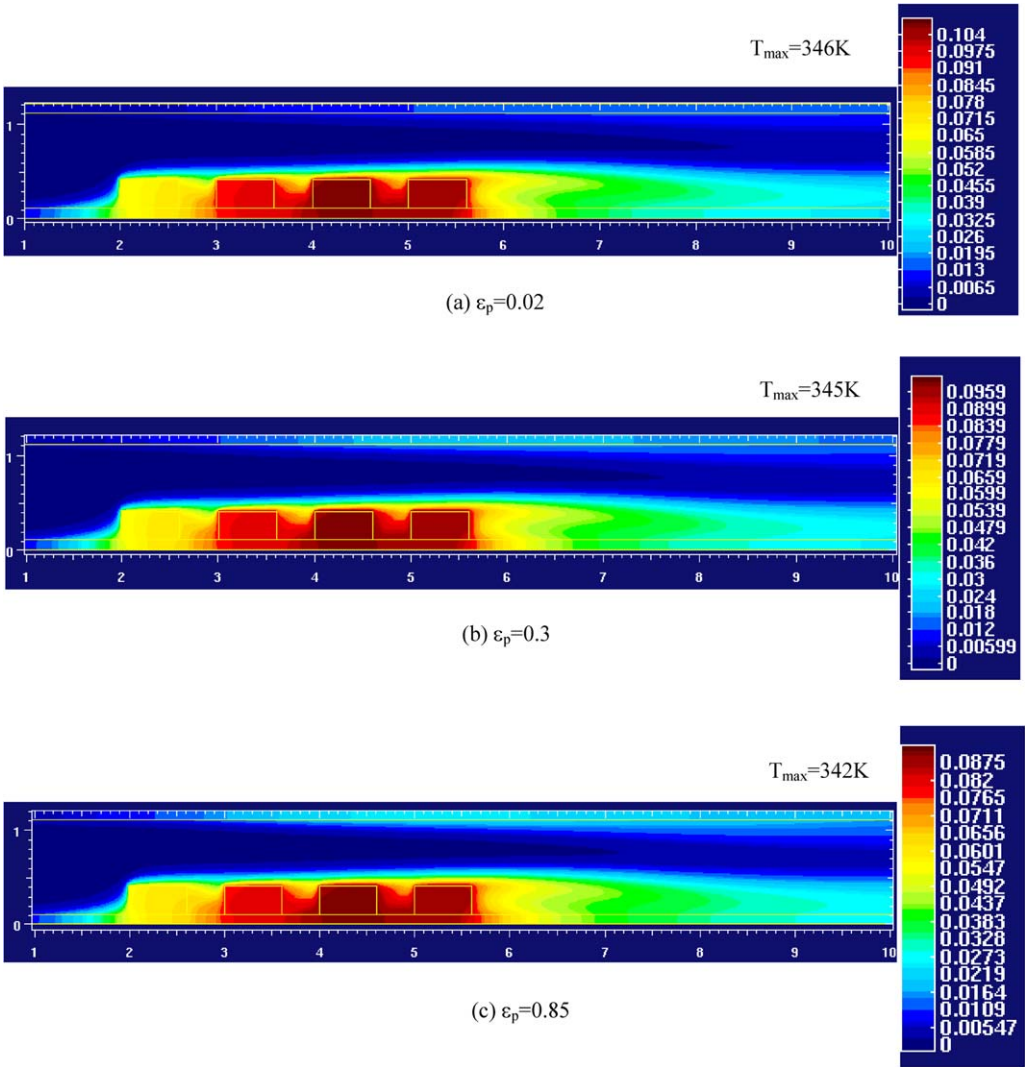

Fig. 8. Effect of the emissivity of the heat source (ε_p) on the temperature distribution at $Re_S = 500$, $Gr_S^* = 8.65 \times 10^5$, $q_v = 1 \times 10^5$ W/m^3, $k_s/k_f = 50$, $k_p/k_f = 100$, $\varepsilon_s = 0.55$.

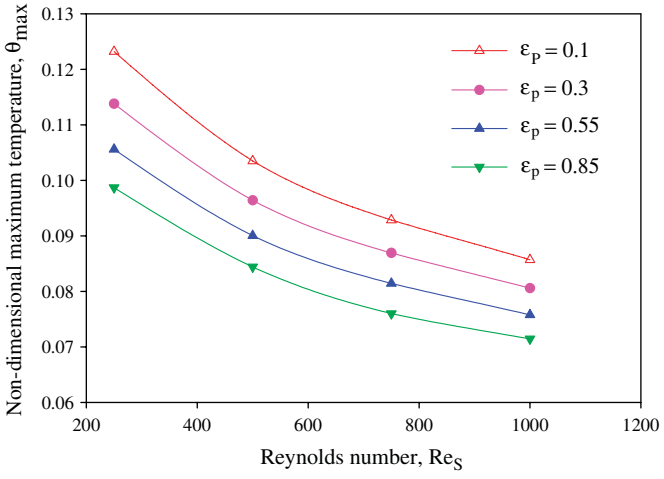

Fig. 9. Effect of the emissivity of the heat sources (ε_p) on the non-dimensional maximum temperature at $Re_S = 250$, 500, 750 and 1000. $Gr_S^* = 8.65 \times 10^5$, $q_v = 1 \times 10^5$ W/m^3, $k_p/k_f = 100$, $k_s/k_f = 50$, $\varepsilon_s = 0.55$.

3.6. Effects of ratio of conductivity of heat sources and thermal conductivity of fluid

As expected, the non-dimensional temperatures decrease as the thermal conductivities of the protruding heat source and substrate increase. The change in the non-dimensional maximum temperature is almost linear when k_p/k_f is varied from 50 to 500.

The change in non-dimensional temperature with respect to the variables $(Re_S/Re_{S,ref})^{0.2}$, $Gr_S^*/Gr_{S,ref}^*$, $((k_p/k_f)/(k_p/k_f)_{ref})^{0.6}$, $((k_s/k_f)/(k_s/k_f)_{ref})^{0.6}$, $(\varepsilon_p/\varepsilon_{p,ref})^{0.65}$ and $(\varepsilon_s/\varepsilon_{s,ref})^{0.56}$ is shown in Fig. 13. The gradient in non-dimensional temperature decreases in all the heat sources as the thermal conductivity of the heat source increases. At $k_p/k_f = 500$, the heat sources become isothermal. The temperature distribution at the interface between the heat source and fluid is shown in Fig. 14 and it is seen that the trends are similar.

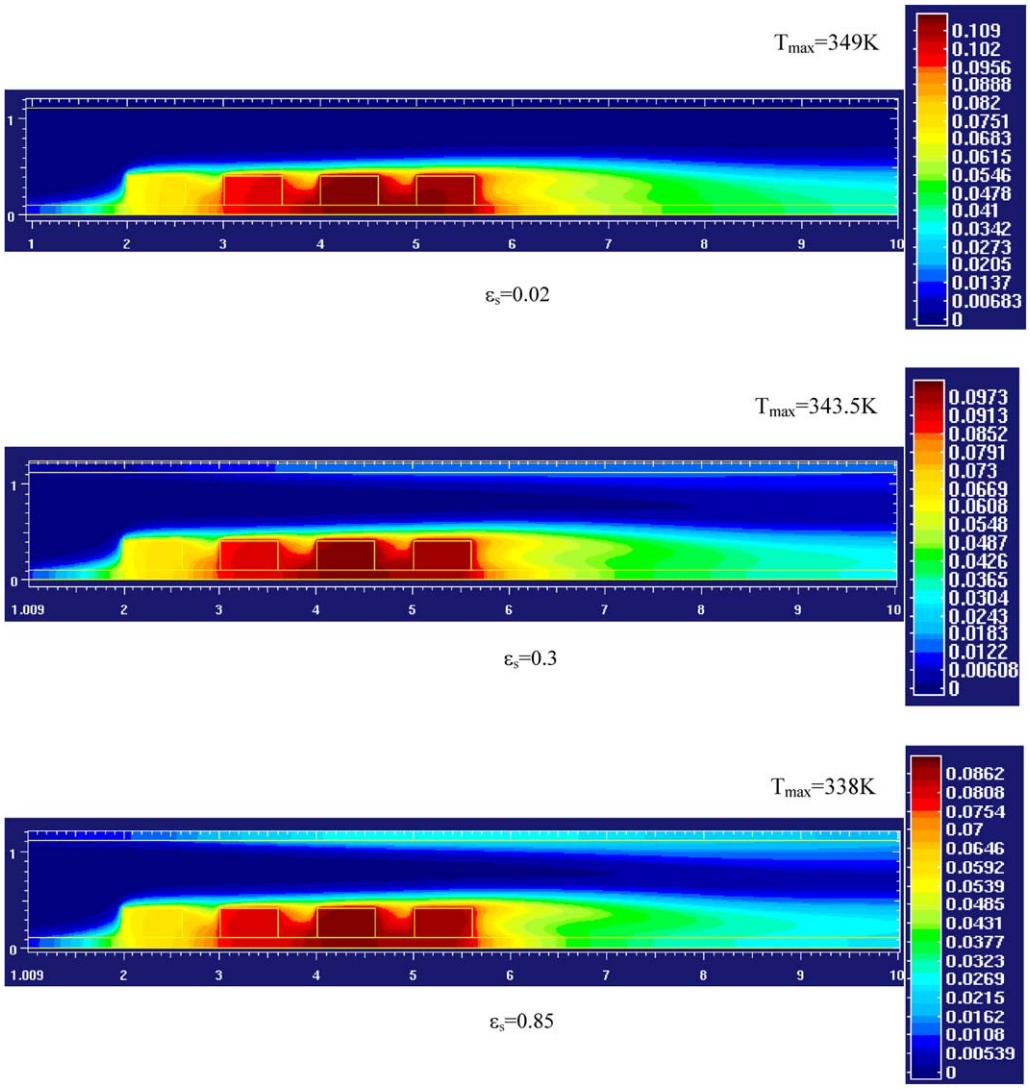

Fig. 10. Effect of the emissivity of the channel wall (ε_s) on the temperature distribution at $Re_S = 500$, $Gr_S^* = 8.65 \times 10^5$, $q_v = 1 \times 10^5$ W/m^3, $k_p/k_f = 100$, $k_s/k_f = 50$, $\varepsilon_p = 0.55$.

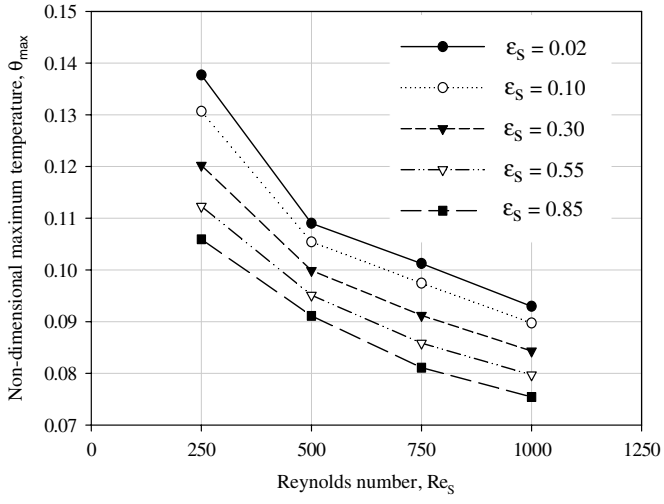

Fig. 11. Effect of emissivity of the channel walls (ε_s) on the non-dimensional maximum temperature at $Re_S = 250$, 500, 750 and 1000 for $Gr_S^* = 8.65 \times 10^5$, $q_v = 1 \times 10^5$ W/m^3, $k_p/k_f = 100$, $k_s/k_f = 50$, $\varepsilon_s = 0.55$.

3.7. Effect of ratio of conductivity of channel walls and thermal conductivity of fluid

The effect of the ratio of the thermal conductivity of the channel walls to the working fluid on the heat transfer characteristics has also been investigated. Fig. 15 shows the effect of thermal conductivity ratio, k_s/k_f on the temperature distribution. It reveals that the temperature of the bottom wall is higher for $k_s/k_f = 500$ compared to $k_s/k_f = 50$ through out the length excluding the position where the third heat source is mounted. As the thermal conductivity of the bottom channel wall increases, the axial conduction also increases and much of the heat is carried away by the working fluid by convection and radiation from the wall portions where the heat sources are not mounted.

The change in non-dimensional maximum temperature corresponding to changes in k_s/k_f and k_p/k_f from 50 to 500 is around 20%. Hence, the conductivity of substrate

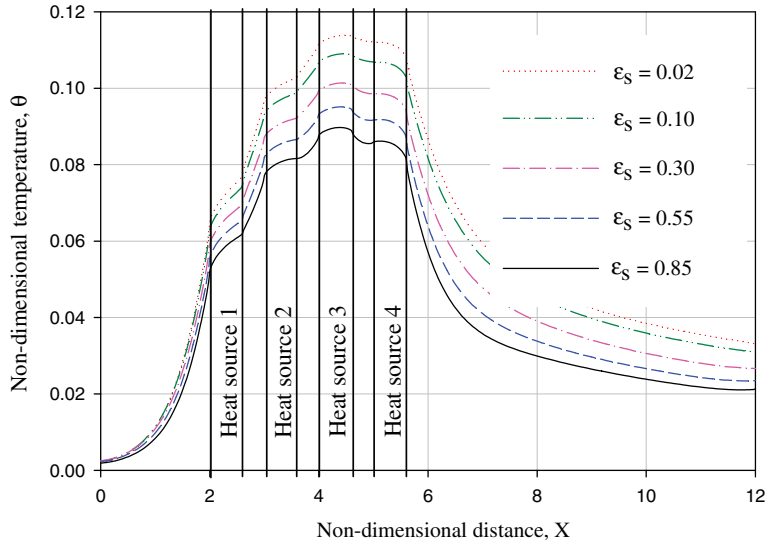

(a)

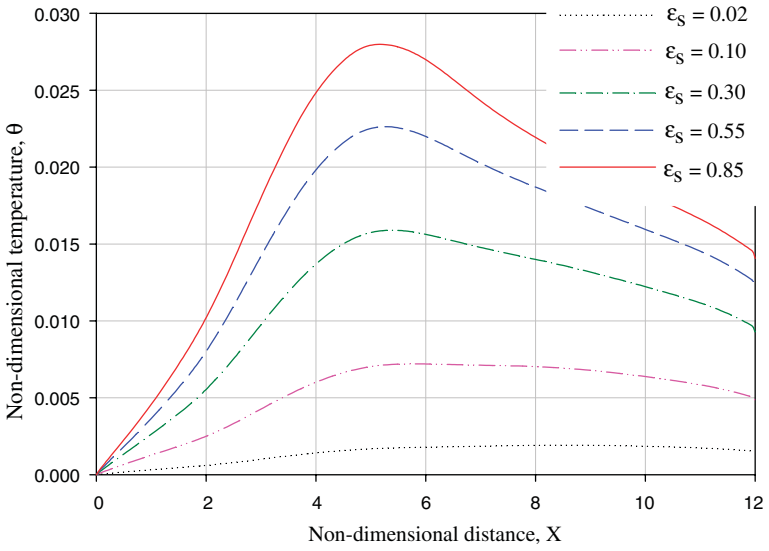

(b)

Fig. 12. Effect of the emissivity of the channel walls (ε_s) on the interface temperature distribution at $Re_S = 500$, $Gr_S^* = 8.65 \times 10^5$, $q_v = 1 \times 10^5$ W/m^3, $k_p/k_f = 100$, $k_s/k_f = 50$, $\varepsilon_p = 0.55$: (a) top surface of the bottom wall; (b) interface between top channel wall and fluid.

and the conductivity of protruding heat source play a significant role in determining the temperature distribution in the channel compared to other parameters.

3.8. Contribution of convection and radiation to heat transfer

The relative contributions of convection and radiation are checked for changes in the emissivity of the heat sources and the channel walls. Fig. 16 shows the relative contribution of radiation compare to convection with the emissivity of heat sources. Other values are at values, viz $Gr_S^* = 8.65 \times 10^5$, $q_v = 1 \times 10^5$ W/m, $k_s/k_f = 50$, $k_p/k_f = 100$, $\varepsilon_s = 0.55$, excluding the emissivity of heat sources which is varied from 0.02 to 0.85. At $Re_S = 250$, when $\varepsilon_p = 0.02$, the contribution by radiation is 10.5% while for $\varepsilon_p = 0.85$, it is 19%. At $Re_S = 1000$, the radiation fraction to total heat transfer is not significant.

For low values of substrate emissivity, the channel walls are highly reflective and much of the radiation heat transfer from the heat sources is reflected to the atmosphere. As the emissivity of channel wall increases, because of increase in radiation interaction, the top cold wall temperature increases and the heat transfer from the channel wall increases. Principally, due to increase in radiation induced convection, the percentage contribution of radiation heat transfer decreases and the contributions of convection heat transfer increases. The relative contributions to the heat transfer by convection and radiation for various emissivities of channel wall (ε_s) and Reynolds numbers are shown in Fig. 17.

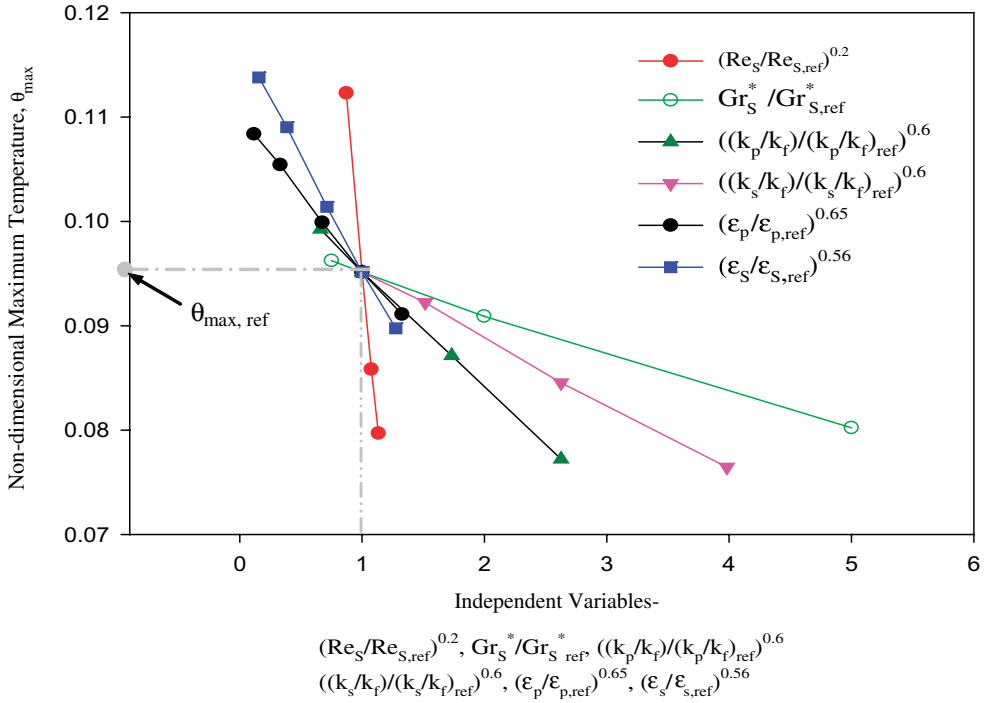

Fig. 13. The variation of non-dimensional maximum temperature with the various independent variables.

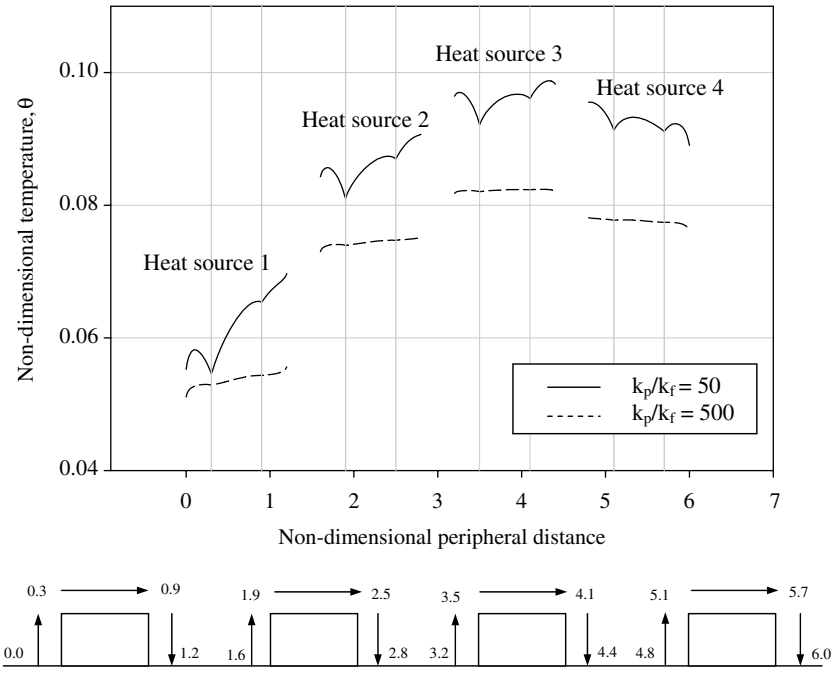

Fig. 14. The effect of k_p/k_f on the interface temperature distribution $Re_S = 500$, $Gr_S^* = 8.65 \times 10^5$, $q_v = 1 \times 10^5$ W/m^3, $k_s/k_f = 50$, $\varepsilon_p = 0.55$, $\varepsilon_s = 0.55$.

3.9. Correlation for the non-dimensional maximum temperature

One of the main objectives in the design of the cooling systems for electronic components is the reduction of the maximum temperature of the electronic components, to ensure reliable operation. Hence, it is desirable to develop a correlation for the maximum temperature attained in the electronic components, rather than a correlation for the average Nusselt number. As previously mentioned, when the geometric and thermal parameters are more, an asymptotic expansion method will help one get a correlation based on fewer data.

The asymptotic expansion approach involves the expansion of the solution to the problem around a particular solution which is taken as the reference solution. A detailed

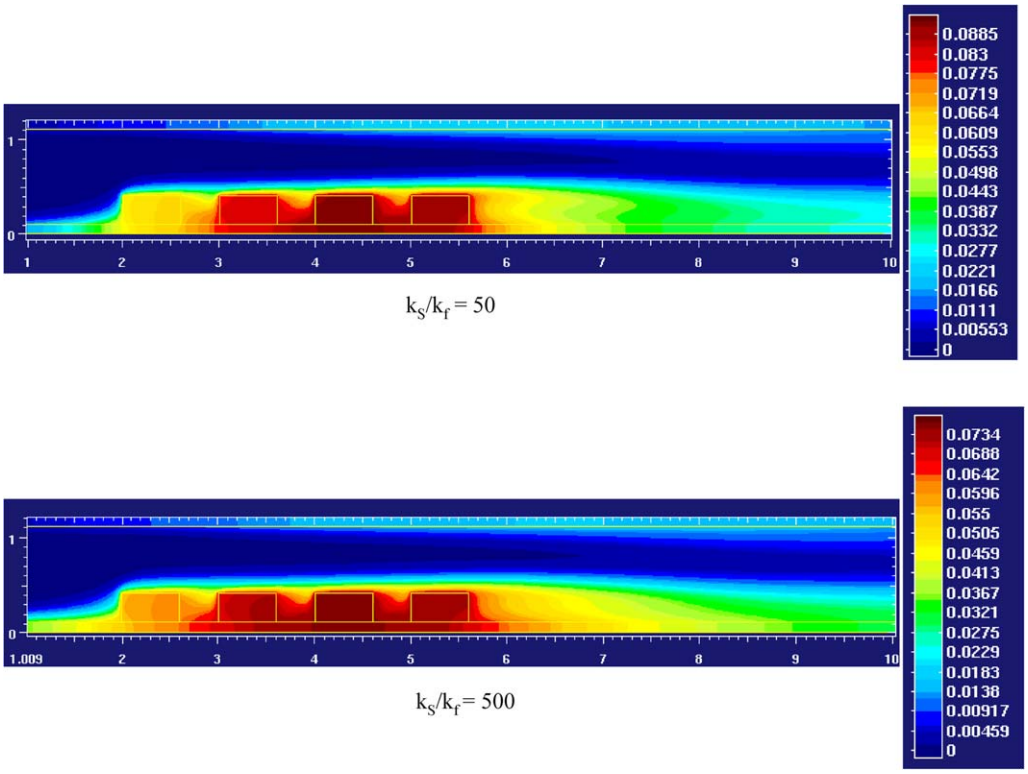

Fig. 15. Effect of the ratio of the thermal conductivity of the substrate to the thermal conductivity of the fluid on the temperature distribution at $Re_S = 500$, $Gr_S^* = 8.65 \times 10^5$, $q_v = 1 \times 10^5$ W/m^3, $k_p/k_f = 100$, $\varepsilon_p = 0.55$, $\varepsilon_s = 0.55$.

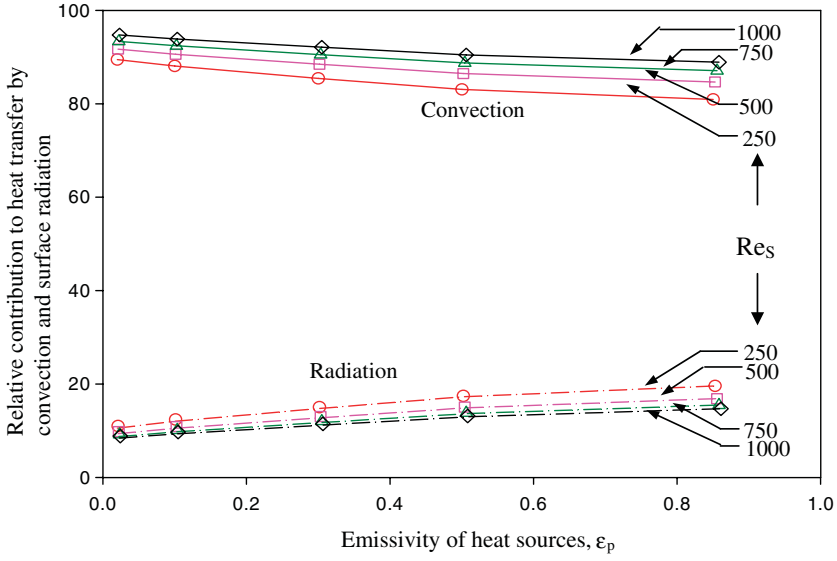

Fig. 16. Variation of the relative contribution to the heat transfer by convection and surface radiation with the emissivity of the heat source (ε_p).

procedure of this method is presented in Balaji and Herwig [20]. The independent variables identified for the present study are Re_S, Gr_S^*, k_p/k_f, k_s/k_f, ε_p and ε_s. The reference values chosen for the expansion are $Re_S = 500$, $Gr_S^* = 8.65 \times 10^5$, $k_p/k_f = 100$, $k_s/k_f = 50$, $\varepsilon_p = 0.55$ and $\varepsilon_s = 0.55$. The θ_{max} for this reference set of parameters is 0.0951. The change in non-dimensional temperature with respect to the variables $(Re_S/Re_{S,ref})^{0.2}$, $Gr_S^*/Gr_{S,ref}^*$, $((k_p/k_f)/(k_p/k_f)_{ref})^{0.6}$, $((k_s/k_f)/(k_s/k_f)_{ref})^{0.6}$, $(\varepsilon_p/\varepsilon_{p,ref})^{0.65}$, $(\varepsilon_s/\varepsilon_{s,ref})^{0.56}$ is shown in Fig. 13.

From this figure, it is clear that a linear expansion is sufficient for all the above-mentioned variables:

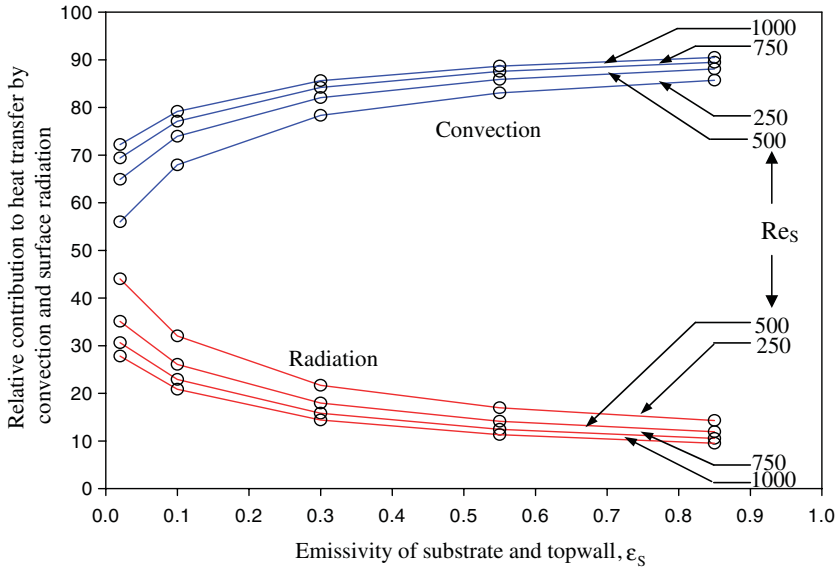

Fig. 17. Variation of the relative contribution to the heat transfer by convection and surface radiation with the emissivity of the substrate (ε_s).

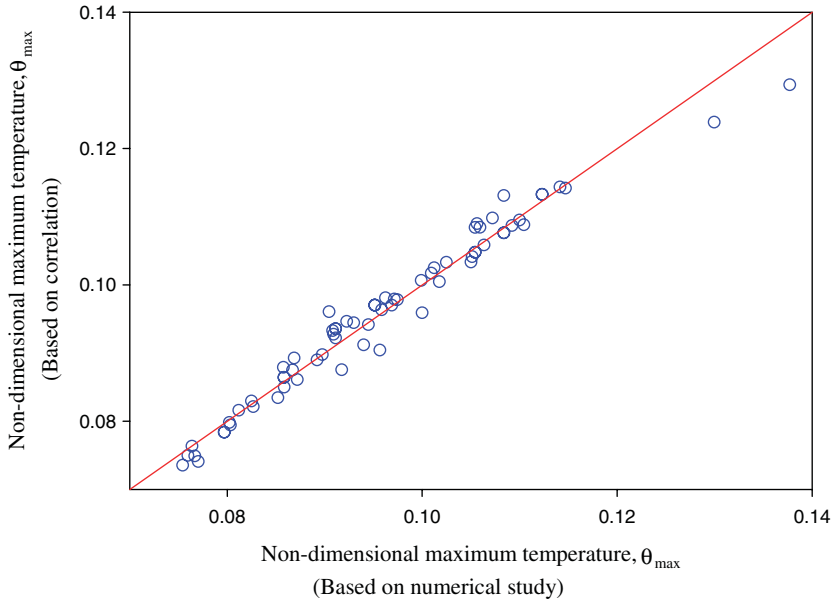

Fig. 18. Comparison of non-dimensional maximum temperature (numerical) with non-dimensional maximum temperature (correlation).

$$\theta_{max} = \theta_{max,ref} + (\phi_1 - \phi_{1,ref})\frac{\partial\theta_{max}}{\partial\phi_1} + (\phi_2 - \phi_{2,ref})\frac{\partial\theta_{max}}{\partial\phi_2} + (\phi_3 - \phi_{3,ref})\frac{\partial\theta_{max}}{\partial\phi_3} + (\phi_4 - \phi_{4,ref})\frac{\partial\theta_{max}}{\partial\phi_4} + (\phi_5 - \phi_{5,ref})\frac{\partial\theta_{max}}{\partial\phi_5} + (\phi_6 - \phi_{6,ref})\frac{\partial\theta_{max}}{\partial\phi_6} \quad (18)$$

where $\phi_1 = (Re_S/Re_{S,ref})^{0.2}$, $\phi_2 = (\varepsilon_s/\varepsilon_{s,ref})^{0.56}$, $\phi_3 = (\varepsilon_p/\varepsilon_{p,ref})^{0.65}$, $\phi_4 = ((k_p/k_f)/(k_p/k_f)_{ref})^{0.6}$, $\phi_5 = ((k_s/k_f)/(k_s/k_f)_{ref})^{0.6}$, $\phi_6 = Gr^*_S/Gr^*_{S,ref}$.

The coefficients $\partial\theta_{max}/\partial\phi_1$, $\partial\theta_{max}/\partial\phi_2$, $\partial\theta_{max}/\partial\phi_3$, $\partial\theta_{max}/\partial\phi_4$, $\partial\theta_{max}/\partial\phi_5$ and $\partial\theta_{max}/\partial\phi_6$ are evaluated one at a time by obtaining the solution to the governing equations with all but one parameter fixed at the reference values. For example, to evaluate $\partial\theta_{max}/\partial\phi_1$, a solution is obtained for $\phi_1 \neq 1.0$ while other variables are fixed at reference values. Following a similar procedure all the other coefficients are calculated. Substituting these values into Eq. (18), one can obtain a correlation for the non-dimensional maximum temperature:

$$\theta_{max} = 0.0951 - 0.123(\phi_1 - 1) - 0.0195(\phi_2 - 1) - 0.0123(\phi_3 - 1) - 0.0109(\phi_4 - 1) - 0.00565(\phi_5 - 1) - 0.0042(\phi_6 - 1) \quad (19)$$

The parity plot (Fig. 18) shows that the non-dimensional maximum temperature obtained using the correlation

compares well within ±5% of the values obtained by the numerical study.

4. Conclusions

The results of a numerical investigation of conjugate mixed convection with surface radiation from a horizontal channel with four discrete heat sources mounted on the bottom channel wall have been presented. The effect of Re_S, Gr_S^*, ε_p, ε_s, k_p/k_f and k_s/k_f on heat transfer and fluid flow characteristics have been analyzed.

Based on the parametric study, the following conclusions are arrived at:

1. The non-dimensional temperature decreases non-linearly as the Reynolds number increases. The effect of radiation interaction also decreases as the Reynolds number increases.
2. As the modified Grashof number increases, the non-dimensional temperature decreases linearly. This shows that the effect of buoyancy is negligible for the range of parameters analyzed in the present study.
3. As k_p/k_f and k_s/k_f increases, the non-dimensional maximum temperature decreases. There is a 20% drop in non-dimensional maximum temperature when the thermal conductivity ratios change from 50 to 500.
4. As the emissivity of the protruding heat source and substrate increase the non-dimensional maximum temperature decreases. The radiation contribution increases from 12% to 20%, as the emissivity of protruding heat source increases from 0.1 to 0.85 at $Re_S = 250$.
5. While carrying out a thermal analysis of a stack of circuit boards with electronic chips (discrete heat sources), the consideration of radiation heat transfer is absolutely essential to accurately predict the non-dimensional maximum temperature.
6. It is possible to develop a reasonably accurate correlation for θ_{max} with limited data, based on the method of asymptotic expansions.

References

[1] J. Davalath, Y. Bayazitoglu, Forced convection cooling across rectangular blocks, ASME J. Heat Transfer 109 (1987) 321–328.
[2] S.H. Kim, A.K. Anand, Laminar developing flow and heat transfer between a series of parallel plates with surface mounted discrete heat sources, Int. J. Heat and Mass Transfer 37 (1994) 2231–2244.
[3] T.J. Young, K. Vafai, Convective flow and heat transfer in a channel containing multiple heated obstacles, Int. J. Heat and Mass Transfer 41 (1998) 3279–3298.
[4] T. Furukawa, W. Yang, Thermal fluid-flow in parallel boards with heat generating blocks, Int. J. Heat and Mass Transfer 46 (2003) 5005–5015.
[5] S.Y. Kim, H.J. Sung, J.M. Hyun, Mixed convection from multiple-layer boards with cross-stream periodic boundary conditions, Int. J. Heat and Mass Transfer 35 (1992) 2941–2952.
[6] T.F. Smith, C. Beckermnn, S.W. Weber, Combined conduction, natural convection, and radiation heat transfer in an electronic chassis, ASME J. Electron. Packag. 113 (1991) 382–391.
[7] S. Lee, J.R. Culham, M.M. Yovanovich, Parametric investigation of conjugate heat transfer from microelectronic circuit boards under mixed convection cooling, in: International Electronic Packaging Conference, San Diego, CA, September 15–19, 1991, pp. 421–446.
[8] C. Balaji, S.P. Venkateshan, Combined conduction, convection and radiation in a slot, cavity, Int. J. Heat and Fluid Flow 14 (1995) 260–267.
[9] A.A. Dehghan, M. Behnia, Numerical investigation of natural convection in a vertical slot with two heat source elements, Int. J. Heat and Fluid Flow 17 (1996) 474–482.
[10] E. Yu, Y.K. Joshi, Heat transfer in discretely heated side-vented compact enclosures by combined conduction, natural convection, and radiation, ASME J. Heat Transfer 121 (1999) 1002–1010.
[11] V.H. Adams, Y. Joshi, D.L. Blackburn, Three-dimensional study of combined conduction, radiation, and natural convection from discrete heat sources in a horizontal narrow-aspect-ratio enclosure, ASME J. Heat Transfer 121 (1999) 992–999.
[12] Y. Liu, N. Phan-Thien, A complete conjugate convection and radiation problem for a heated block in a vertically heated square enclosure, Comput. Mech. 24 (1999) 175–186.
[13] C. Gururaja Rao, C. Balaji, S.P. Venkateshan, Effect of radiation conjugate mixed convection in a vertical channel with a discrete heat source in each wall, Int. J. Heat and Mass Transfer 45 (2002) 3331–3347.
[14] A.T. Joseph, S.P. Venkateshan, G. Kuruvilla, Experimental studies on cooling of electronic components in a channel, Int. J. Transport Phenom. 3 (2001) 103–118.
[15] H.C. Hottel, A.F. Saroffim, Radiative Heat Transfer, McGraw Hill, New York, 1967.
[16] S.V. Patankar, Numerical Heat Transfer and Fluid Flow, Hemisphere, New York, 1980.
[17] D.A. Kaminski, C. Prakash, Conjugate natural convection in a square enclosure: effect of conduction in one of the vertical walls, Int. J. Heat and Mass Transfer 29 (1986) 1979–1988.
[18] B. Premachandran, C. Balaji, Mixed convection heat transfer from a horizontal channel with protruding heat sources, Heat and Mass Transfer 41 (2004) 510–518.
[19] N. Ramesh, W. Merzkirch, Combined convection and radiation heat transfer in side-vented open cavities, Int. J. Heat and Fluid Flow 22 (2001) 180–187.
[20] C. Balaji, H. Herwig, The use of ACFD approach in problems involving surface radiation and free convection, Int. Commun. Heat and Mass Transfer 30 (2003) 251–259.